

**This is an electronic reprint of the original article.
This reprint *may differ* from the original in pagination and typographic detail.**

Author(s): Vasdev, Neil; Moran, Matthew; Chirakal, Raman; Tuononen, Heikki; Suontamo, Reijo; Bain, Alex; Schrobilgen, Gary

Title: NMR Spectroscopic Evidence for the Intermediacy of XeF₃⁻ in XeF₂/F⁻ Exchange, Attempted Syntheses and Thermochemistry of XeF₃⁻ Salts, and Theoretical Studies of the XeF₃⁻ Anion

Year: 2010

Version:

Please cite the original version:

Vasdev, N., Moran, M., Chirakal, R., Tuononen, H., Suontamo, R., Bain, A., & Schrobilgen, G. (2010). NMR Spectroscopic Evidence for the Intermediacy of XeF₃⁻ in XeF₂/F⁻ Exchange, Attempted Syntheses and Thermochemistry of XeF₃⁻ Salts, and Theoretical Studies of the XeF₃⁻ Anion. *Inorganic Chemistry*, 49(19), 8997-9004.
<https://doi.org/10.1021/ic101275m>

All material supplied via JYX is protected by copyright and other intellectual property rights, and duplication or sale of all or part of any of the repository collections is not permitted, except that material may be duplicated by you for your research use or educational purposes in electronic or print form. You must obtain permission for any other use. Electronic or print copies may not be offered, whether for sale or otherwise to anyone who is not an authorised user.

**NMR Spectroscopic Evidence for the Intermediacy of XeF_3^-
in XeF_2/F^- Exchange, Attempted Syntheses and Thermochemistry of XeF_3^- Salts,
and Theoretical Studies of the XeF_3^- Anion**

**Neil Vasdev,^{†,‡} Matthew D. Moran,[†] Heikki M. Tuononen,[§] Raman Chirakal,^{†,‡}
Reijo J. Suontamo,[§] Alex D. Bain,[†] and Gary J. Schrobilgen^{†,*}**

[†] Department of Chemistry, McMaster University, Hamilton, Ontario L8S 4M1, Canada;

[‡] Department of Nuclear Medicine, McMaster University Medical Centre and Hamilton
Health Sciences, Hamilton, Ontario L8N 3Z5, Canada; [§] University of Jyväskylä, P.O.
Box 35, FIN-40014, Jyväskylä, Finland

*Author to whom correspondence should be addressed. E-mail: schrobil@mcmaster.ca

Abstract

The existence of the trifluoroxenate(II) anion, XeF_3^- , had been postulated in a prior NMR study of the exchange between fluoride ion and XeF_2 in CH_3CN solution. The enthalpy of activation for this exchange, ΔH^\ddagger , has now been determined by use of single selective inversion ^{19}F NMR spectroscopy to be $74.1 \pm 5.0 \text{ kJ mol}^{-1}$ (0.18M) and $56.9 \pm 6.7 \text{ kJ mol}^{-1}$ (0.36 M) for equimolar amounts of $[\text{N}(\text{CH}_3)_4][\text{F}]$ and XeF_2 in CH_3CN solvent. Although the XeF_3^- anion has been observed in the gas phase, attempts to prepared the Cs^+ and $\text{N}(\text{CH}_3)_4^+$ salts of XeF_3^- have been unsuccessful, and are attributed to the low fluoride ion affinity of XeF_2 and fluoride ion solvation in CH_3CN solution. The XeF_3^- anion would represent the first example of an AX_3E_3 VSEPR arrangement of electron lone pair and bond pair domains. Fluoride-ion exchange reactions between XeF_2 and the F^- anion have been probed computationally using CCSD and DFT (PBE1PBE) methods. The energy-minimized geometry of the ground state shows that the F^- anion is only weakly coordinated to XeF_2 ($\text{F}_2\text{Xe}\cdots\text{F}^-$; distorted Y-shape possessing C_s symmetry), while the XeF_3^- anion exists as a first-order transition state in the fluoride-ion exchange mechanism, and is planar and Y-shaped (C_{2v} symmetry). The molecular geometry and bonding for the XeF_3^- anion has been described and rationalized in terms of electron localization function (ELF) calculations, as well as the VSEPR model of molecular geometry. Quantum-chemical calculations at the CCSD/aVTZ level of theory, using a continuum solvent model (CH_3CN), accurately reproduced the transition-state enthalpy observed by ^{19}F NMR spectroscopy, and shows a negative but negligible enthalpy for the formation of the $\text{F}_2\text{Xe}\cdots\text{F}^-$ adduct in this medium.

Introduction

Of the binary xenon fluorides, only XeF_4 and XeF_6 are known to form anionic salts with fluoride ion donors. Xenon tetrafluoride behaves as a weak fluoride ion acceptor (calculated gas-phase fluoride ion affinity (FIA), $247.3 \text{ kJ mol}^{-1}$)¹ towards alkali metal fluorides and the naked fluoride ion source $[\text{N}(\text{CH}_3)_4][\text{F}]$ to give salts of the pentagonal planar XeF_5^- anion.² Xenon hexafluoride is a considerably stronger fluoride ion acceptor (FIA, $313.8 \text{ kJ mol}^{-1}$),¹ forming the XeF_7^- and XeF_8^{2-} anions with alkali metal (Na, K, Rb, Cs) fluorides.^{3,4} In addition to the alkali metal fluoride salts, the NO^+ and NO_2^+ salts have been prepared by direct reaction of XeF_6 with NOF or NO_2F , namely, $[\text{NO}_2][\text{XeF}_7]$,⁵ $[\text{NO}]_2[\text{XeF}_8]$,^{6,7} and $[\text{NO}_2][\text{Xe}_2\text{F}_{13}]$.⁵ The $[\text{NO}]_2[\text{XeF}_8]$ salt was shown, by single-crystal X-ray diffraction, to contain the slightly distorted square antiprismatic XeF_8^{2-} anion.^{6,7} Xenon hexafluoride also reacts with $[\text{NF}_4][\text{HF}_2]$ in anhydrous hydrogen fluoride (aHF) to give $[\text{NF}_4][\text{XeF}_7]$, which was converted to $[\text{NF}_4]_2[\text{XeF}_8]$ by selective laser photolysis and characterized by vibrational spectroscopy.⁸ The XeF_7^- and $\text{Xe}_2\text{F}_{13}^-$ anions have also been characterized by X-ray crystallography as their Cs^+ and NO_2^+ salts.⁵ The XeF_7^- anion has a monocapped octahedral structure, while the $\text{Xe}_2\text{F}_{13}^-$ anion may be described as an XeF_6 molecule bridged by two long Xe–F bonds to an XeF_7^- anion such that the bridging fluorines avoid the axial nonbonding electron pair of the XeF_6 molecule.

In contrast, XeF_2 has not been conclusively shown by experiment to exhibit fluoride-ion acceptor properties in solution or in the solid state (FIA, 83.3 kJ mol^{-1}).¹ The trifluoroxenate(II) anion, XeF_3^- , was first proposed to be a plausible anionic noble-gas species based on well-known diagonal trends within the Periodic Table.⁹ The XeF_3^- anion was later proposed as an intermediate in the “base-catalyzed” fluorination of SO_2 by XeF_2 ,¹⁰ however, reasonable alternative mechanisms were subsequently proposed for this reaction which did not involve this anion.¹¹ Experimental evidence for the XeF_3^- anion has been obtained in the gas phase from the

negative ion mass spectra of XeF_2 ¹² and XeOF_4 ,¹³ and from energy-resolved collision-induced dissociation studies of XeF_2 .¹⁴ The related XeF_3^\bullet radical has recently been stabilized in an argon matrix and characterized by Fourier-transform infrared spectroscopy and explored by kinetic measurements.¹⁵ Radiochemical experiments using ^{18}F (half life = 109.7 min) have failed to confirm fluoride-ion exchange with XeF_2 in water,¹⁶ CH_2Cl_2 ,¹⁷ or CH_3CN solvents.¹⁷ However, $^{18}\text{F}^-$ exchanges between $[^{18}\text{F}]\text{-HF}$, $[^{18}\text{F}]\text{-SiF}_4$, and $[^{18}\text{F}]\text{-AsF}_5$ and XeF_2 have been successfully used for the preparation of $[^{18}\text{F}]\text{-XeF}_2$ (through XeF^+ and Xe_2F_3^+ as intermediates),¹⁸ that was, in turn, used for the preparation of $[^{18}\text{F}]\text{-2-fluoro-2-deoxy-D-glucose}$ ¹⁹ and $[^{18}\text{F}]\text{-6-fluoro-L-3,4-dihydroxyphenylalanine}$.²⁰ Computational chemistry has more recently been employed to study the nature of the XeF_3^- anion in the gas phase,^{1,14} as well as the thermodynamics of its formation (for details see Computational Results).¹⁴

In an earlier study, the authors observed exchange between F^- and XeF_2 in CH_3CN solvent under rigorously anhydrous conditions by use of 2-D $^{19}\text{F}\text{-}^{19}\text{F}$ EXSY experiments.¹⁷ Fluorine-19 exchange occurred between the “naked” fluoride-ion source, $[\text{N}(\text{CH}_3)_4][\text{F}]$, and XeF_2 in CH_3CN solvent at 15 °C, providing the first conclusive evidence for XeF_2/F^- exchange on the NMR timescale.¹⁷ The ^{19}F exchange was postulated to proceed through the formation of XeF_3^- (eq 1).



The objectives of the present study are to better define the nature of the XeF_2/F^- exchange, using single selective inversion NMR and to establish the fluoride ion acceptor properties of XeF_2 by attempting the syntheses of representative salts containing the XeF_3^- anion. Computational methods (CCSD and DFT) have also been used to explore the nature of the XeF_2/F^- exchange. The current study also clarifies inconsistencies that have arisen in recent computational studies relating to the structure of the XeF_3^- anion.^{1,14}

Results and Discussion

Intermolecular Exchange Between F⁻ and XeF₂. Although EXSY experiments are very effective for determining connectivities among exchanging sites, one-dimensional, single selective inversion experiments are considered to be superior for the study of slow exchange processes and for probing the thermodynamics of the transition states.²¹ The enthalpy of activation, ΔH^\ddagger , for intermolecular ¹⁹F exchange between fluoride ion and XeF₂ was determined from two samples containing equimolar amounts of [N(CH₃)₄][F] and XeF₂ in CH₃CN solvent (0.18 and 0.36 M), in conjunction with single selective inversion NMR spectroscopic experiments conducted at variable temperatures. Figure 1 shows the results of a ¹⁹F selective inversion experiment acquired at -15 °C for a 0.18 M sample of XeF₂ and [N(CH₃)₄][F] in CH₃CN solvent using various delay times. The analysis of this intermolecular exchange process was carried out over the temperature range -40 to 0 °C, and the data were fit (Figure 2), yielding a ΔH^\ddagger value of 74.1 ± 5.0 kJ mol⁻¹. A more concentrated sample (0.36 M XeF₂ and [N(CH₃)₄][F] in CH₃CN solvent) was similarly analyzed over the temperature range -35 to -15 °C, yielded a ΔH^\ddagger value of 56.9 ± 6.7 kJ mol⁻¹. Because the two values are not statistically different (to within ±3σ) within the concentration and temperature ranges amenable for study by NMR spectroscopy, the values can be averaged (65.5 ± 8.4 kJ mol⁻¹) and are indicative of a single transition state (see Computational Results). The presence of HF₂⁻ in the samples (Figure 2), as seen previously,¹⁷ results from F⁻ or XeF₂ attack on the solvent to produce HF which, in turn, reacts with F⁻ to form HF₂⁻. The former and predominant reaction occurs by abstraction of H⁺ from CH₃CN by F⁻,²² and by reaction of XeF₂ with CH₃CN.²³ The HF₂⁻ anion was not found to exchange with XeF₂ by single selective inversion NMR spectroscopy (Figure 2) or by 2-D ¹⁹F-¹⁹F EXSY.¹⁷

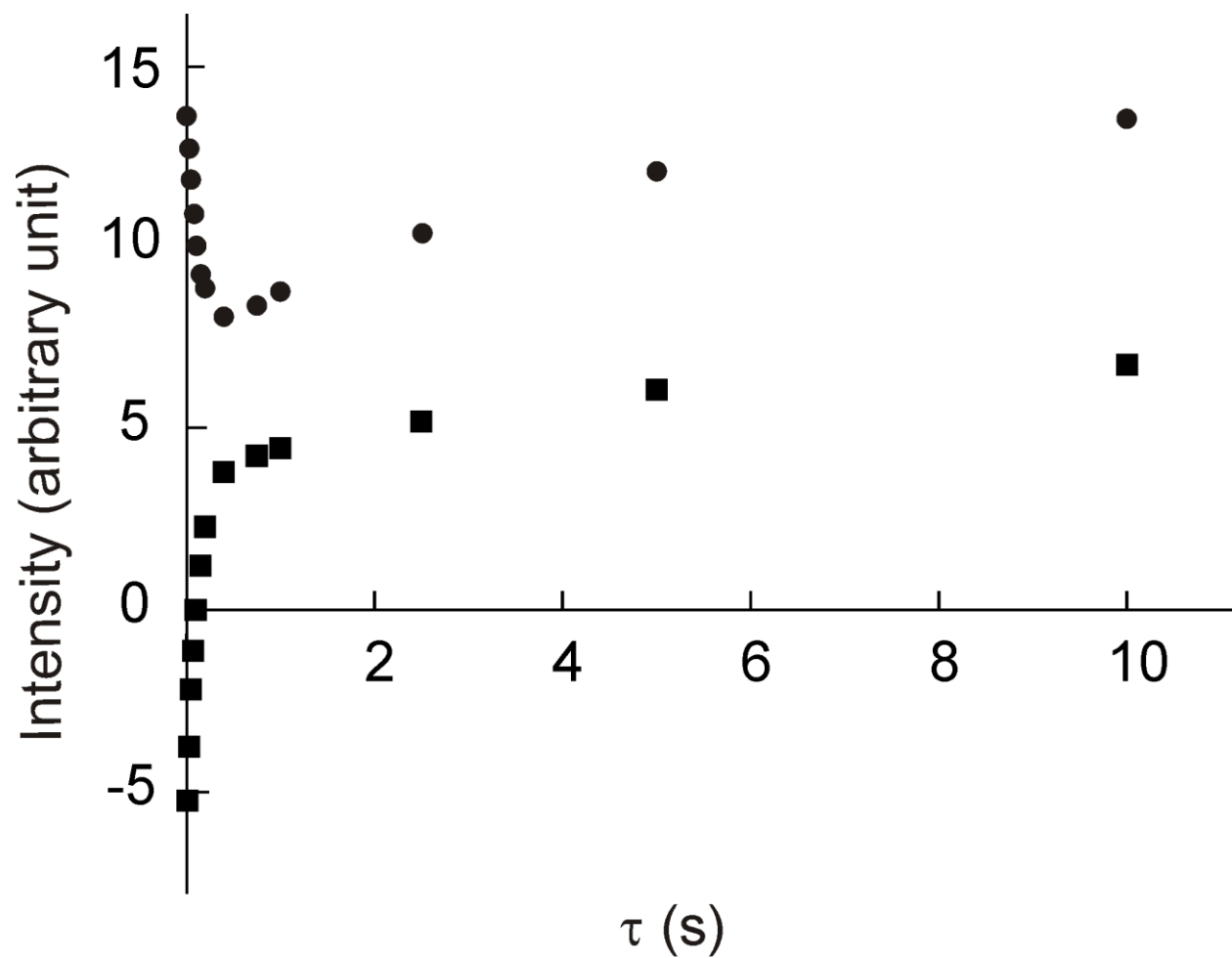


Figure 1. The enthalpy of activation, ΔH^\ddagger , determined by use of single selective inversion ^{19}F NMR spectroscopy to be $74.1 \pm 5.0 \text{ kJ mol}^{-1}$ from a stoichiometric sample (0.18 M in both $[\text{N}(\text{CH}_3)_4][\text{F}]$ and XeF_2 in CH_3CN solvent at -15°C) of XeF_2 (●) and F^- (■).

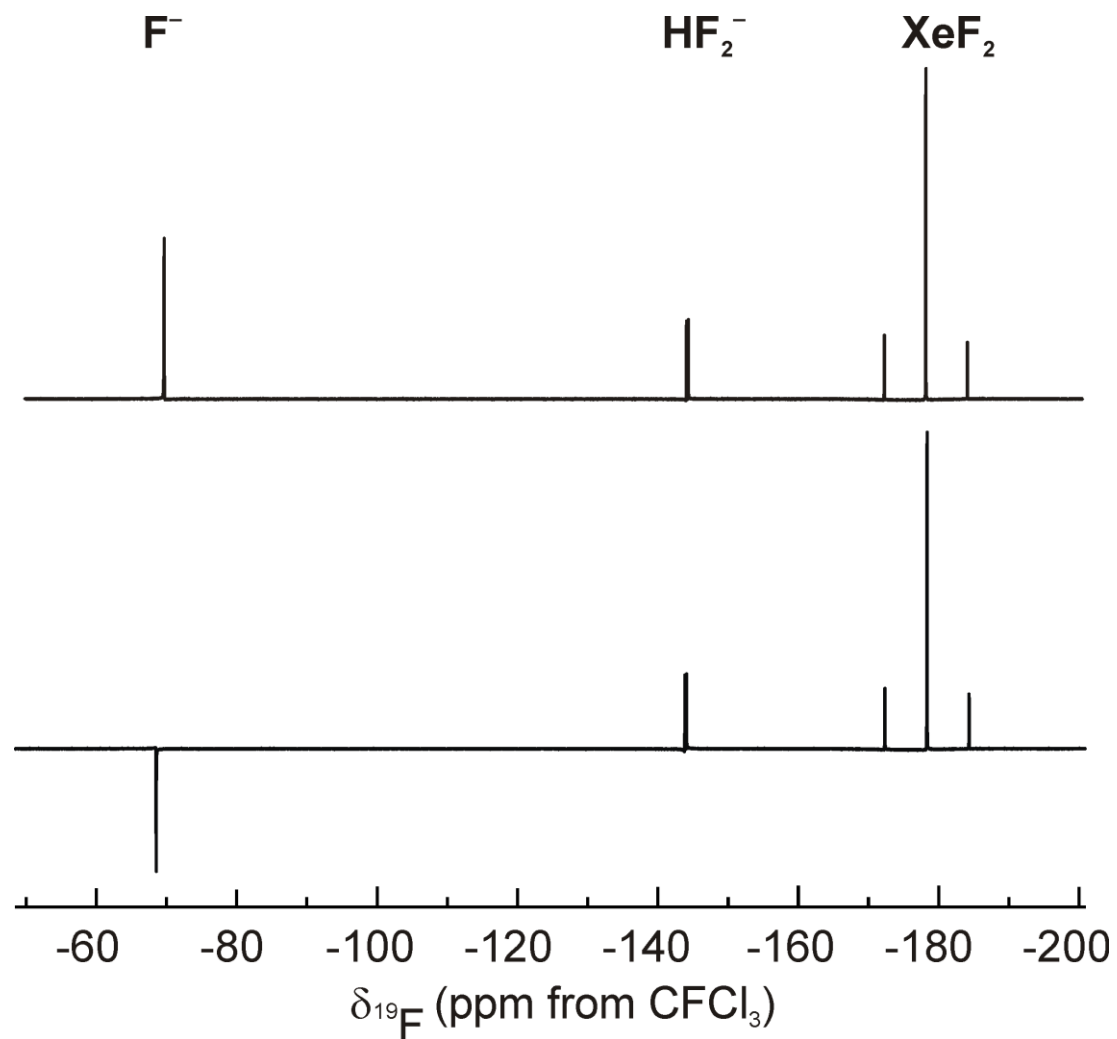


Figure 2. The ^{19}F NMR resonances of XeF_2 , $[\text{N}(\text{CH}_3)_4][\text{F}]$, and $[\text{N}(\text{CH}_3)_4][\text{HF}_2]$ in CH_3CN solvent ($-15\text{ }^\circ\text{C}$). The 1-D NMR spectrum of XeF_2 and its natural abundance ^{129}Xe satellites and F^- (top trace) and the full-observed relaxation under the combined influence of spin-lattice relaxation and chemical exchange that results in the selective inversion of F^- with respect to XeF_2 .

Attempted Syntheses of the Cs⁺ and N(CH₃)₄⁺ Salts of XeF₃⁻. In attempts to synthesize [N(CH₃)₄][XeF₃], stoichiometric amounts of XeF₂ and [N(CH₃)₄][F] were dissolved in CH₃CN solvent by briefly warming the mixture to room temperature, and in CHF₃ solvent at 0 °C (12 h) under autogeneous pressure in a heavy-wall glass vessel. The Raman spectra of both samples were recorded at -160 °C under the frozen solvents and after solvent removal. Only bands arising from unreacted starting materials were observed, demonstrating that no XeF₃⁻ salts had formed based on calculated vibrational frequencies and Raman intensities of XeF₃⁻ (Table S1 in the Supporting Information). The inability to form a salt of the XeF₃⁻ anion in either CHF₃ or CH₃CN solvents parallels failed attempts to form [N(CH₃)₄][F₃] from F₂ and [N(CH₃)₄][F] in CH₃CN and CHF₃ solvents,²⁴ and was attributed to the high solvation energies of the fluoride ion in these polar solvents.

The syntheses of the Cs⁺ and N(CH₃)₄⁺ salts containing the XeF₃⁻ anion were also attempted in the absence of a solvent. Fusion of a four-fold molar excess of XeF₂ with CsF resulted in no reaction up to 170 °C. When a six-fold molar excess of XeF₂ with respect to [N(CH₃)₄][F] was slowly heated to the melting point of XeF₂ (129 °C), rapid oxidative fluorination of the N(CH₃)₄⁺ cation ensued with detonation of the sample. The inability to form salts of the XeF₃⁻ anion prompted thermochemical and computational studies to investigate the formation of XeF₃⁻ in the solid state, gas phase, and in CH₃CN solution.

Thermochemistry. To account for failed attempts to prepare either the Cs⁺ or N(CH₃)₄⁺ salt of the XeF₃⁻ anion, quantum-chemical calculations and established semi-empirical methods²⁵⁻²⁹ were used in conjunction with known thermodynamic quantities to estimate $\Delta H^\circ_{\text{rxn}}$, $\Delta S^\circ_{\text{rxn}}$, and $\Delta G^\circ_{\text{rxn}}$ for eq 1 in the absence of a solvent. The standard enthalpies for the reactions were determined by analyzing their Born-Fajans-Haber cycles (eq 2). The enthalpy change for the gas-

phase reaction (eq 3) corresponds to the negative of the fluoride ion affinity (FIA) of XeF₂. A prior reported fluoride ion affinity value of 83.3 kJ mol⁻¹ has been used.¹ The experimental

$$\Delta H^{\circ}_{\text{rxn}}([\text{M}][\text{XeF}_3]) = H^{\circ}_{\text{L}}([\text{M}][\text{F}]) + \Delta H^{\circ}(\text{XeF}_2)_{\text{sub}} - \text{FIA}(\text{XeF}_2) - \Delta H^{\circ}_{\text{L}}([\text{M}][\text{XeF}_3]) \quad (2)$$



value for the enthalpy of sublimation ($\Delta H^{\circ}(\text{XeF}_2)_{\text{sub}}$) for XeF₂ (55.71 kJ mol⁻¹) was used.³⁰ The lattice enthalpies of [M][F] and [M][XeF₃] were estimated by use of the volume-based method of Bartlett et al.^{25,26} as generalized by Jenkins et al.^{27,28} in eq 4, where *R* is the gas constant (8.314 J K⁻¹mol⁻¹), *I* is the ionicity of the salt and the constants, α , β , and *p*, depend on the nature of the

$$\Delta H^{\circ}_{\text{L}} = 2I \left(\frac{\alpha}{\sqrt[3]{V_m}} + \beta \right) + pRT \quad (4)$$

salt. For the salts under investigation, which are singly charged and non-linear, the following values were used: *I* = 1, α = 117.3 mm kJ mol⁻¹, β = 51.9 kJ mol⁻¹, and *p* = 2. In this formalism, $\Delta H^{\circ}_{\text{L}}$ is the lattice enthalpy and is defined as the energy required to break the crystal lattice, and therefore has a positive value. The volume-based approach is particularly useful because the formula unit volume (*V_m*) of an unknown salt can be estimated with reasonable accuracy using several methods.^{27,31} In the present case, $V_m([\text{M}][\text{XeF}_3]) = V_m(\text{XeF}_2) + V_m([\text{M}][\text{F}])$, where $V_m(\text{XeF}_2) = 0.0622 \text{ nm}^3$, $V_m([\text{Cs}][\text{F}]) = 0.0573 \text{ nm}^3$, and $V_m([\text{N}(\text{CH}_3)_4][\text{F}]) = 0.1460 \text{ nm}^3$, giving $V_m([\text{Cs}][\text{XeF}_3]) = 0.1195 \text{ nm}^3$ and $V_m([\text{N}(\text{CH}_3)_4][\text{XeF}_3]) = 0.2082 \text{ nm}^3$. The calculated lattice enthalpies are:

$$\Delta H^{\circ}_{\text{L}}([\text{Cs}][\text{F}]) = 717 \text{ kJ mol}^{-1}$$

$$\Delta H^{\circ}_{\text{L}}([\text{N}(\text{CH}_3)_4][\text{F}]) = 554 \text{ J kJ mol}^{-1}$$

$$\Delta H^{\circ}_{\text{L}}([\text{Cs}][\text{XeF}_3]) = 585 \text{ kJ mol}^{-1}$$

$$\Delta H^{\circ}_{\text{L}}([\text{N}(\text{CH}_3)_4][\text{XeF}_3]) = 505 \text{ kJ mol}^{-1}$$

and net enthalpies (eq 2) calculated for the reactions of [M][F] (M = N(CH₃)₄, Cs) with XeF₂ under standard conditions are:

$$\Delta H^{\circ}_{\text{rxn}}([\text{Cs}][\text{XeF}_3]) = 105 \text{ kJ mol}^{-1}$$

$$\Delta H^{\circ}_{\text{rxn}}([\text{N}(\text{CH}_3)_4][\text{XeF}_3]) = 22 \text{ kJ mol}^{-1}$$

A method for estimating the absolute standard entropy of a salt from its unit volume has been reported by Jenkins and Glasser (eq 5) where $k = 1360 \text{ JK}^{-1} \text{ mol}^{-1} \text{ nm}^{-3} (\text{formula unit})^{-1}$

$$S^\circ = kV_m + c \quad (5)$$

and $c = 15 \text{ J mol}^{-1} \text{ K}^{-1}$.²⁹ The standard entropies for the $[\text{M}][\text{F}]$ and $[\text{M}][\text{XeF}_3]$ are:

$$S^\circ([\text{Cs}][\text{F}]) = 92.9 \text{ J mol}^{-1} \text{ K}^{-1} \quad S^\circ([\text{N}(\text{CH}_3)_4][\text{F}]) = 213.5 \text{ J mol}^{-1} \text{ K}^{-1}$$

$$S^\circ([\text{Cs}][\text{XeF}_3]) = 177.5 \text{ J mol}^{-1} \text{ K}^{-1} \quad S^\circ([\text{N}(\text{CH}_3)_4][\text{XeF}_3]) = 298.2 \text{ J mol}^{-1} \text{ K}^{-1}$$

When coupled with the experimental standard entropies of $\text{XeF}_{2(\text{s})}$ ($115.09 \text{ J mol}^{-1} \text{ K}^{-1}$),³⁰ this method allows $\Delta S^\circ_{\text{rxn}}$ (eq 6) and $\Delta G^\circ_{\text{rxn}}$ (eq 7) to be calculated for the reactions of interest.

$$\Delta S^\circ_{\text{rxn}}([\text{M}][\text{XeF}_3]) = S^\circ([\text{M}][\text{XeF}_3]) - S^\circ(\text{XeF}_2) - S^\circ([\text{M}][\text{F}]) \quad (6)$$

$$\Delta G^\circ_{\text{rxn}}([\text{M}][\text{XeF}_3]) = \Delta H^\circ_{\text{rxn}}([\text{M}][\text{XeF}_3]) - T\Delta S^\circ_{\text{rxn}}([\text{M}][\text{XeF}_3]) \quad (7)$$

The $\Delta S^\circ_{\text{rxn}}$ and $\Delta G^\circ_{\text{rxn}}$ values obtained for these reactions are:

$$\Delta S^\circ_{\text{rxn}}([\text{Cs}][\text{XeF}_3]) = -30.5 \text{ J mol}^{-1} \text{ K}^{-1} \quad \Delta S^\circ_{\text{rxn}}([\text{N}(\text{CH}_3)_4][\text{XeF}_3]) = -30.4 \text{ J mol}^{-1} \text{ K}^{-1}$$

$$\Delta G^\circ_{\text{rxn}}([\text{Cs}][\text{XeF}_3]) = 114 \text{ kJ mol}^{-1} \quad \Delta G^\circ_{\text{rxn}}([\text{N}(\text{CH}_3)_4][\text{XeF}_3]) = 31 \text{ kJ mol}^{-1}$$

The reaction enthalpies and Gibbs free energies are positive indicating that both reactions are endothermic and non-spontaneous under standard conditions. As expected, the reaction employing the larger $\text{N}(\text{CH}_3)_4^+$ cation is far less endothermic and closer to spontaneity.

Computational Results. It was first suggested that the XeF_3^- anion would have an octahedral (meridional) AX_3E_3 (A = central atom, X = bonded electron pair, E = valence electron lone pair) VSEPR arrangement of bonded pairs and valence electron lone pairs (T-shaped geometry).⁹ Although the *mer*-isomer of XeF_3^- anion minimizes the lone pair-lone pair repulsions, there are no examples known in which three valence electron lone pairs are positioned at approximately 90° to one another. Because the XeF_3^- anion has thus far eluded solid-state characterization, computational chemistry was employed to help elucidate its structure in the gas phase as well as in CH_3CN solution through employment of a continuum solvent model. The thermodynamic

properties of XeF_3^- , XeF_2 , and F^- were also computed for comparison with the experimentally determined transition-state energy for the formation of the anion from XeF_2 and F^- in CH_3CN ($\Delta H^\ddagger = 65.5 \pm 8.4 \text{ kJ mol}^{-1}$).

To fully appreciate the complexity of this seemingly simple system, it is important to distinguish the two, discrete forms of the anion that have stationary points on the potential energy surface (PES), as computed in the present work and in previous studies:^{1,14} a planar, distorted Y-shaped anion (C_s symmetry, Figure 3a) possessing two short Xe–F bonds and one long Xe–F bond (which is still within the sum of the van der Waals radii of xenon and fluorine, 3.63 \AA ³²), and a planar, Y-shaped anion (C_{2v} symmetry, Figure 3b) possessing three similar Xe–F bond lengths. The former will be referred to as the $\text{F}_2\text{Xe}\cdots\text{F}^-$ adduct, while the latter will be referred to as the XeF_3^- anion. A third, T-shaped adduct of C_{2v} symmetry was also computed as

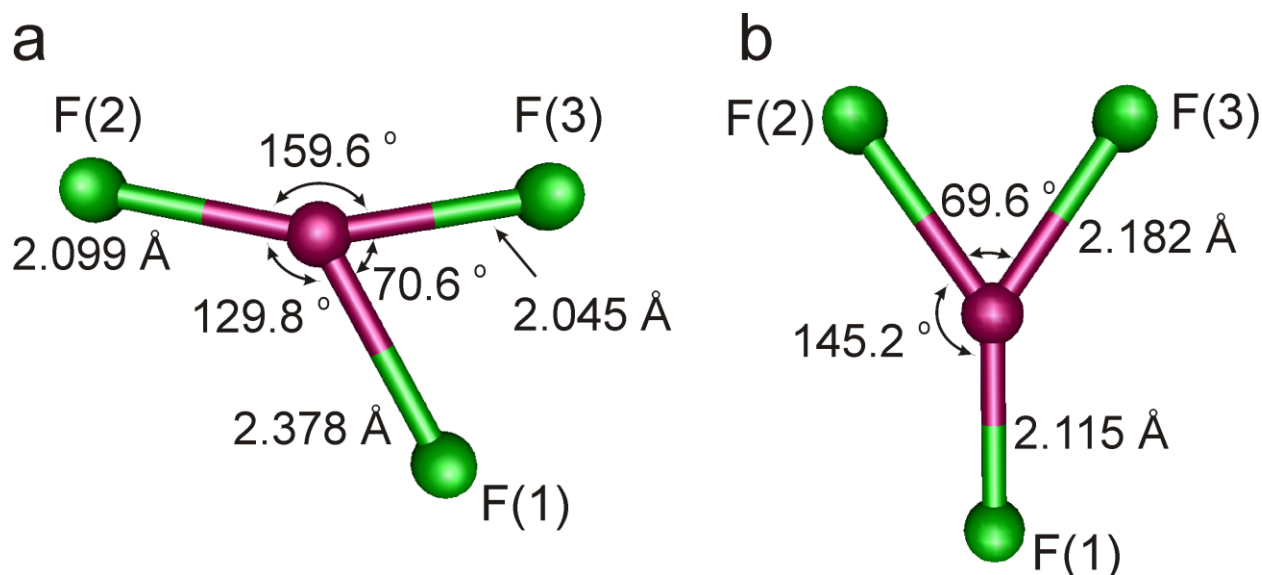


Figure 3. Calculated gas-phase geometries (PBE1/aVTZ) of (a) the $\text{F}_2\text{Xe}\cdots\text{F}^-$ adduct (ground state, C_s symmetry), and (b) the XeF_3^- anion (transition state, C_{2v} symmetry).

a stationary point on the PES,^{1,14} but it was found that a slight, symmetry-lowering distortion to C_s symmetry gave the lower energy, ground-state structure, which is, in fact, the *mer*-structure

(albeit with one long Xe---F interaction). Finally, a Y-shaped anion (D_{3h}) was also computed as a diradical species, in accord with the structure predicted by MO theory,¹⁴ but was found to be 59.8 to 110.0 kJ mol⁻¹ higher in energy than the ground-state structure.

(a) Electronic Structures of the XeF₃⁻ and F₂Xe---F⁻ Anions. (i) In the Gas Phase.

The optimized geometries of the XeF₃⁻¹⁴ and F₂Xe---F⁻^{1,14} anions have recently been reported; the results, along with the present work, are summarized in Table 1. In the former report, DFT calculations with the B3LYP functional indicated that the XeF₃⁻ anion (C_{2v}) is the energy-minimized structure (all frequencies real, Table S1 in the Supporting Information) when either an all-electron Maroulis basis set or an ECP basis set (SDB-cc-pVTZ) is used for xenon.¹⁴ The F₂Xe---F⁻ adduct (C_{2v}) was higher in energy relative to the XeF₃⁻ anion by ca. 2.1–15.1 kJ mol⁻¹,¹⁴ and is a transition state (one imaginary frequency). However, the previous work¹⁴ overlooked a lower-energy, ground-state conformation of the F₂Xe---F⁻ adduct possessing a lower symmetry (C_s), as found in the latter study (4.85 kJ mol⁻¹ lower than the C_{2v} structure at the CCSD(T)/aVTZ level of theory).¹ Although the bond lengths for the adduct are incorrectly reported in the text, they are correct in the Supporting Information.¹ The latter bond lengths and angles are in good agreement with the bond lengths calculated for the F₂Xe---F⁻ adduct in this study (Table 1). Furthermore, the existence of the XeF₃⁻ anion as a transition state was not explored.¹

Calculations performed in the present work (DFT using the PBE1 functional, and CCSD; basis sets: aVTZ (for F) and aVTZ(-PP) (for Xe) were done without symmetry constraints, and reveal that the global-energy minimum of the anion is the F₂Xe---F⁻ adduct (C_s symmetry), in

Table 1. Calculated^a Gas-Phase and Solution-Phase (CH₃CN)^b Geometries for the XeF₃⁻ and F₂Xe---F⁻ Anions

	XeF ₃ ⁻			F ₂ Xe---F ⁻			
	gas phase (C _{2v})	CH ₃ CN (C _{2v})	ref. 14 (C _{2v}) ^c	bond lengths (Å)			
				gas phase (C _s)	CH ₃ CN (C _s)	ref. 14 (C _{2v}) ^c	ref. 1 (C _s) ^d
Xe-F(1)	2.084 (2.115)	2.026 (2.067)	2.161	2.567 (2.378)	3.035 (3.112)	2.681	2.510
Xe-F(2)	2.153 (2.182)	2.207 (2.230)	2.233	2.037 (2.099)	1.990 (2.009)	2.064	2.073
Xe-F(3)	2.153 (2.182)	2.207 (2.230)	2.233	1.970 (2.045)	1.983 (2.000)	2.064	2.002
				bond angles (°)			
F(1)-Xe-F(2)	145.4 (145.2)	145.9 (146.0)	145.1	116.9 (129.8)	99.2 (99.2)	94.5	121.0
F(1)-Xe-F(3)	145.4 (145.2)	145.9 (146.0)	145.1	74.0 (70.6)	82.4 (82.6)	94.5	72.4
F(2)-Xe-F(3)	69.1 (69.6)	68.2 (68.1)	69.8	169.1 (159.6)	178.3 (178.2)	171.0	166.6

^a CCSD/aug-cc-pVTZ(-PP) (PBE1PBE/aug-cc-pVTZ(-PP) values in parentheses). ^b Values were computed using the CPCM solvent model. ^c Using the B3LYP functional with aug-cc-pVTZ basis set for F and SDB-cc-pVTZ basis set for Xe. ^d CCSD(T)/aug-cc-pVTZ.

accord with the CCSD(T) results reported in the Supporting Information of reference 1 (Table 1, Figure 3a). For the DFT structure, one of the Xe–F bonds is distinctly longer (2.378 Å) than the other two (2.045 and 2.099 Å), but well within the sum of the van der Waals radii for Xe and F. The F–Xe–F fragment is slightly bent (159.6°) so that the structure can be viewed as XeF₂ perturbed by a fluoride ion, in agreement with the previous work.¹ Although the qualitative agreement with the geometries optimized at the DFT and CCSD levels is good, the geometric parameters (Table 1) show that the PBE1 functional predicts a structure in which F(1) is more strongly bound to the XeF₂ fragment, whereas the coupled-cluster method predicts a significantly longer Xe–F(1) bond length (2.561 Å) and a more open F(2)–Xe–F(3) bond angle (169.1°).

In order to elucidate the structure of the transition state, a scan involving the step-wise reduction in the long Xe–F bond length of the F₂Xe---F⁻ adduct was computed. In both cases (PBE1 and CCSD), the transition-state structure was that of the Y-shaped XeF₃⁻ anion (Figure 3b). The structures thus obtained were further optimized as transition states at their respective levels of theory (Table 2). Calculations were also performed to determine if the T-shaped, C_{2v}-symmetric transition state was a potential, competing transition state. The C_{2v}-symmetric transition state was 14.6 (PBE1) and 16.7 (CCSD) kJ mol⁻¹ higher in energy than the Y-shaped XeF₃⁻ anion, indicating that the latter is the more favored transition state. Thermodynamic calculations for the intermolecular exchange between XeF₂ and F⁻ were also reinvestigated in the present work (see Computational Assessment of Intermolecular Exchange).

The transition state (XeF₃⁻) appears to be far more covalently bound than the ground-state F₂Xe---F⁻ adduct; using DFT methods, the XeF₃⁻ anion possesses three similar Xe–F bond lengths (2.115 Å and 2.182 Å (×2)). The two large (145.2°) angles and one small (69.6°) angle allow for the retention of the lone-pair torus around the xenon atom, as shown by ELF analyses (see Electron Localization Function (ELF) Analyses). The structure computed at the

CCSD/aVTZ level of theory was found to possess similar geometric parameters to that of the DFT structure (Table 1). It is unclear why the XeF_3^- anion was computed to be an energy minimum in the previous study¹⁴ since the structure remains a transition state even when the calculations are performed using the same basis set-density functional combination as employed in the original work.

(ii) In CH_3CN Solution. Because of the thermodynamics for the enthalpy of activation of F^- ion exchange with XeF_2 in CH_3CN solvent were found to be in good agreement with the experimental findings (see Computational Assessment of Intermolecular Exchange), the structures for $\text{F}_2\text{Xe}\cdots\text{F}^-$ and XeF_3^- were also determined in CH_3CN (using the CPCM model,³³ Table 1). For the $\text{F}_2\text{Xe}\cdots\text{F}^-$ adduct, the bond between XeF_2 and F^- loses some of its covalent character. The optimized structure contains a near-linear XeF_2 fragment (PBE1, 178.2° ; CCSD, 178.3°) with a long Xe-F bond equal to 3.112 \AA (PBE1) and 3.035 \AA (CCSD) that is still within the sum of the Xe and F van der Waals radii. Unlike the gas-phase structures, the geometric parameters in CH_3CN solution do not change significantly between PBE1 and CCSD (Table 1), and show that the interaction between XeF_2 and F^- is primarily electrostatic in nature, precluding the observation of an $\text{F}_2\text{Xe}\cdots\text{F}^-$ adduct by ^{19}F NMR spectroscopy in this solvent or by low-temperature Raman spectroscopy in frozen CH_3CN solution. In contrast to the adduct, the geometry for the XeF_3^- anion modeled in CH_3CN solution remains essentially unchanged from that determined in the gas phase (Table 1).

(b) Computational Assessment of Intermolecular Exchange between Fluoride Ion and XeF_2 . **(i) In the Gas Phase.** In light of the ^{19}F NMR spectroscopic study (see Intermolecular Exchange Between Fluoride Ion and XeF_2), the reaction between XeF_2 and F^- was modeled by a series of computational scans with optimizations of the stationary points (PBE1 and CCSD) to (1) establish the exchange pathway, and (2) determine how well the

calculated thermodynamics agree with the experimental ^{19}F NMR spectroscopic results. Although the energy profile for the direct fluoride ion loss from the XeF_3^- anion was recently calculated at the DFT level,¹⁴ failure to obtain the correct ground-state and transition-state structures (see Electronic Structures of the XeF_3^- and $\text{F}_2\text{Xe}\cdots\text{F}^-$ Anions) led to an erroneous interpretation of the exchange thermodynamics.

The stepwise elongation of the long Xe–F bond of the $\text{F}_2\text{Xe}\cdots\text{F}^-$ adduct (i.e., the FIA) within the C_s symmetry constraint led to a smooth increase in the total energy of the system with an asymptotic (optimized) value of 97.1 kJ mol^{-1} at the PBE1/aVTZ level of theory ($115.3 \text{ kJ mol}^{-1}$ at the CCSD/aVTZ level of theory). The PBE1 energy is in good agreement with the gas-phase enthalpies determined in previous experimental ($81.2 \pm 5.9 \text{ kJ mol}^{-1}$)¹⁴ and theoretical (96.7 ¹⁴ and 83.3 ¹ kJ mol^{-1}) work. Conversely, the stepwise shortening of the long Xe–F bond of the $\text{F}_2\text{Xe}\cdots\text{F}^-$ adduct (i.e., the enthalpy of activation) resulted in the XeF_3^- anion as the transition state. The enthalpy change in going from the ground state to the transition state was small (PBE1, $\Delta H^\ddagger = 1.3 \text{ kJ mol}^{-1}$; CCSD, $\Delta H^\ddagger = 13.4 \text{ kJ mol}^{-1}$). Although the gas-phase results indicate that the FIA of XeF_2 is sufficient to form the $\text{F}_2\text{Xe}\cdots\text{F}^-$ adduct in the solid state, the FIA value is much smaller than those determined for XeF_4 ($247.3 \text{ kJ mol}^{-1}$)¹ and XeF_6 ($313.8 \text{ kJ mol}^{-1}$)¹. Furthermore, the energy barrier to fluoride ion exchange between XeF_2 and F^- (i.e., the formation of the XeF_3^- anion) is very small in contrast with the experimental findings. Therefore, in an attempt to reconcile the experimental and computational findings, the thermodynamics of the XeF_2/F^- exchange were modeled in CH_3CN .

(ii) In CH_3CN Solution. In marked contrast with the gas-phase results, the step-wise elongation of the long Xe–F bond of the $\text{F}_2\text{Xe}\cdots\text{F}^-$ adduct (i.e., the FIA) yielded a much smaller increase in the enthalpy (PBE1, 5.0 kJ mol^{-1} ; CCSD, 7.1 kJ mol^{-1}). The enthalpy of formation from XeF_2 and F^- suggests that XeF_2 possesses little to no affinity for the fluoride ion in CH_3CN

solution. Because the enthalpy of formation is small for the $\text{F}_2\text{Xe}\cdots\text{F}^-$ adduct, the enthalpy for the formation of XeF_3^- (i.e., the enthalpy of activation) could be determined relative to free XeF_2 and F^- , and gave energy barriers for the fluoride ion exchange reaction that were much higher than those in the gas phase: 24.7 (PBE1) and 50.2 kJ mol^{-1} (CCSD). While the value using the PBE1 functional was underestimated, the value obtained using the CCSD method fell within the range of those experimentally determined for the fluoride-ion exchange ($65.5 \pm 8.4 \text{ kJ mol}^{-1}$). Taken as whole, the calculations confirm that the direct reaction between XeF_2 and F^- in solution leads to fluoride ion exchange via a transition state corresponding to the Y-shaped XeF_3^- anion.

Finally, in order to assess the validity of averaging the two activation enthalpies obtained by ^{19}F NMR spectroscopy (i.e., that the two energies did not correspond to two different transition states existing at two different concentrations), other possible transition states on the potential energy surface were explored. Both XeF_4^{2-} and $\text{XeF}_3^-\cdot\text{XeF}_2$ were assessed using the CH_3CN solvent model at both the PBE1/aVTZ and MP2/aVTZ levels of theory, but dissociated to XeF_3^- and F^- and to XeF_3^- and XeF_2 , respectively. These calculations lend further support to the view that the XeF_3^- anion is the only viable transition state in the exchange between XeF_2 and F^- .

(c) Natural Bond Orbital (NBO) Analyses. The results from the NBO analyses conducted for XeF_3^- and $\text{F}_2\text{Xe}\cdots\text{F}^-$ are collected in Table 2. The calculated natural population analysis (NPA) charges for the $\text{F}_2\text{Xe}\cdots\text{F}^-$ adduct (from PBE1 and CCSD geometries, respectively) show that the combined charge of the XeF_2 fragment is near zero ($-0.18/-0.04$), and that the negative charge is distributed unevenly among the three fluorine atoms, with F(1) carrying most of the charge ($-0.82/-0.96$). The most logical Lewis-like depiction of the total electron density given by the NBO analysis shows that bonding in the $\text{F}_2\text{Xe}\cdots\text{F}^-$ adduct has two

Table 2. Gas-Phase and Solution-Phase (CH₃CN)^a NBO Analyses and NPA Charges for the XeF₃⁻ and F₂Xe---F⁻ Anions^b

	XeF ₃ ⁻		F ₂ Xe---F ⁻	
	natural charges			
	gas phase	solution phase	gas phase	solution phase
Xe	1.227 (1.097)	1.242 (1.161)	1.292 (1.130)	1.289 (1.260)
F(1)	-0.720 (-0.684)	-0.661 (-0.654)	-0.956 (-0.817)	-0.996 (-0.995)
F(2)	-0.753 (-0.707)	-0.791 (-0.754)	-0.699 (-0.681)	-0.650 (-0.636)
F(3)	-0.753 (-0.707)	-0.791 (-0.754)	-0.636 (-0.633)	-0.642 (-0.629)
	bond orders			
Xe-F(1)	0.219 (0.255)	0.287 (0.260)	0.020 (0.155)	0.007 (0.011)
Xe-F(2)	0.167 (0.229)	0.169 (0.173)	0.248 (0.259)	0.306 (0.297)
Xe-F(3)	0.167 (0.229)	0.169 (0.173)	0.292 (0.293)	0.310 (0.301)

^a Values were computed using the CPCM solvent model. ^b CCSD/aVTZ//CCSD/aVTZ (PBE1/aVTZ//PBE1/aVTZ in parentheses).

major contributions; a bonding Xe–F interaction within the F(2)–Xe–F(3) fragment (Xe–F bond orders of 0.259/0.248 and 0.293/0.292) and an adduct interaction between neutral XeF₂ and the fluoride ion, F(1) (bond order of 0.155/0.020), which is calculated to be much stronger using DFT methods. Using the solvent model, the bond orders for the DFT and CCSD structures become more similar, with slightly stronger Xe–F(2)/F(3) interactions (0.297/0.312 and 0.301/0.316, respectively) and a much weaker Xe–F(1) interaction (0.011/0.003).

In contrast to the F₂Xe---F⁻ adduct, the XeF₃⁻ anion is a covalently bound Y-shaped anion (C_{2v}), with all the fluorine atoms having similar charges (PBE1: -0.67, -0.71, and -0.71; CCSD: -0.72, -0.75 and -0.75), and also possessing similar bond orders (PBE1: 0.262, 0.204, and 0.204; CCSD: 0.219, 0.167, and 0.167). These values do not change substantially when modeled in CH₃CN solution.

(d) Electron Localization Function (ELF) Analyses. The use of ELF for inorganic systems containing xenon has proven useful for qualitative analysis.³⁴ It is also well known that while ELF analyses can be instructive, there is no direct physical interpretation for an ELF basin or its population.

The linear structure of XeF₂, and its calculated ELF isosurface (performed on the PBE1/VTZ-optimized geometry) shows a torus comprised of the three lone pairs around xenon (Figure 4a). Addition of a fluoride ion results in a distortion of the lone pair torus upon addition of another bonding pair of electrons and an increase in electron-electron repulsion. This repulsion is reduced by lowering the symmetry from C_{2v} to C_s, allowing the fluoride ion to avoid a “head-on” interaction with the electron lone-pair torus (Figure 4b), and keeping the fluoride distance longer than a typical covalent Xe–F bond (Table 1). In contrast to the F₂Xe---F⁻ adduct,

the XeF_3^- anion shows strong covalent bonding for all three fluorine atoms. Where VSEPR would predict a *mer*-arrangement (based on an octahedral arrangement of bond pairs and lone pairs), computations show a highly distorted, planar Y-shaped geometry with C_{2v} symmetry. The ELF analysis (Figure 4c) indicates that the distortion arises from retention of the torus about the xenon atom. In contrast with the $\text{F}_2\text{Xe}\cdots\text{F}^-$ adduct, the torus is slightly distorted towards the F(1) atom, and away from the F(2) and F(3) atoms. It is interesting to note that it is energetically more favorable when two fluorine atoms are 69° away from each other, rather than having three lone pairs at an approximately 90° angle to one another (the meridional structure).

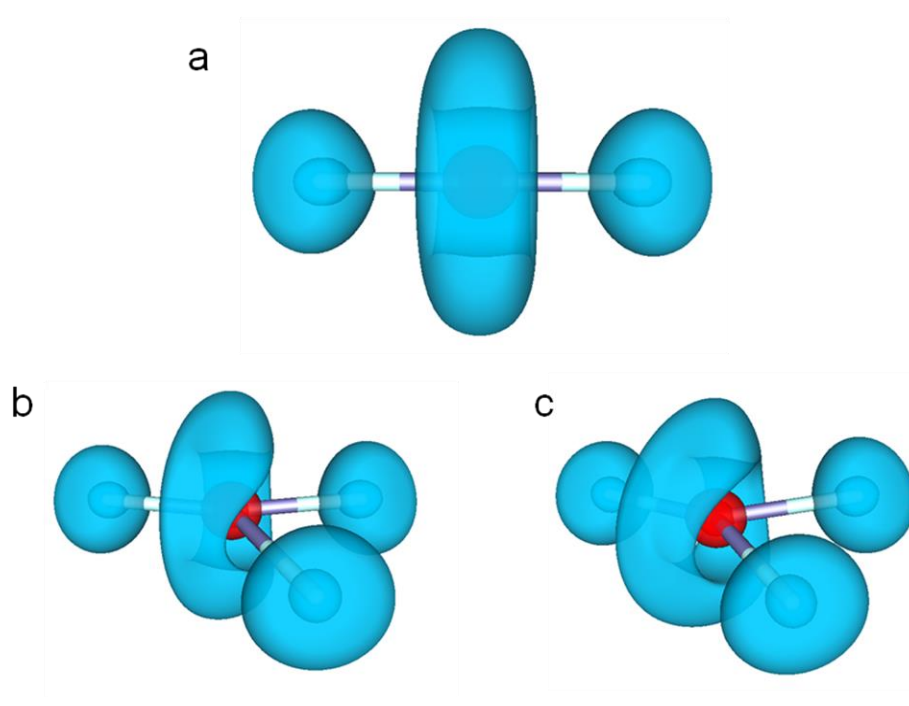


Figure 4. Electron localization function isosurfaces (contour level 0.7) of (a) XeF_2 , (b) the $\text{F}_2\text{Xe}\cdots\text{F}^-$ adduct, and (c) the XeF_3^- anion (calculated at the PBE1/aVTZ level of theory. Color scheme: blue, lone-pair (monosynaptic) basin; red, core basin.

Conclusions

The standard enthalpy of formation for the intermolecular ^{19}F -exchange between XeF_2 and $[\text{N}(\text{CH}_3)_4][\text{F}]$ in CH_3CN solvent was measured by single selective inversion NMR

spectroscopy and determined to be $65.5 \pm 8.4 \text{ kJ mol}^{-1}$. The inability to synthesize salts containing the XeF_3^- anion in the present work is attributed to the low fluoride ion affinity of XeF_2 . The calculated energy-minimized geometries (DFT and CCSD) of the $\text{F}_2\text{Xe}\cdots\text{F}^-$ and XeF_3^- anions show distorted Y-shaped (adduct) and Y-shaped (anion) structures, respectively. Computed enthalpies using the CH_3CN solvent model demonstrated that XeF_2 has no affinity for the fluoride ion in solution, and gave activation enthalpies (CCSD) that agreed well with the experimentally determined activation enthalpy.

Experimental Section

Materials and Synthetic Techniques. Fluoroform, CHF_3 (Canadian Liquid Air, 98%) was handled using a metal vacuum line. Before entering the vacuum manifold, CHF_3 gas was passed through a copper coil cooled to $-78 \text{ }^\circ\text{C}$ in solid dry ice. Preparation of all other starting materials and standard techniques were conducted as previously described,¹⁷ unless otherwise specified.

Attempted Syntheses of Salts Containing the XeF_3^- Anion. Inside a drybox, $[\text{N}(\text{CH}_3)_4][\text{F}]$ (0.01620 g, 0.01739 mmol) and XeF_2 (0.02960 g, 0.01749 mmol) were loaded into a glass thick-wall h-shaped reaction vessel (9-mm o.d., 2.5-mm i.d.). The reaction vessel was attached to a stainless steel vacuum line and anhydrous CHF_3 was condensed into the vessel. Once the reaction vessel was flame sealed it was placed in a dewar containing a 95% ethanol/liquid nitrogen slush at ca. $-110 \text{ }^\circ\text{C}$. The reaction mixture was then agitated over a period of 30 min while warming to $0 \text{ }^\circ\text{C}$ and allowed to stand for 12 h. The sample was mixed again and a Raman spectrum was recorded at $-160 \text{ }^\circ\text{C}$ directly on the thick-walled glass reaction vessel containing the solid sample. The CHF_3 was distilled into one arm of the reaction vessel and was flame sealed off. A white, crystalline powder was obtained and Raman spectra were recorded at -155

°C directly on the sealed off portion of the thick-wall glass reaction vessel containing the solid sample.

Equimolar amounts of $[\text{N}(\text{CH}_3)_4][\text{F}]$ (0.01620 g, 0.1739 mmol) and XeF_2 (0.02960 g, 0.1749 mmol) were also loaded into a ¼-in. glass tube fused to a 5-mm o.d. thick-wall glass NMR tube, inside a drybox. The reaction vessel was attached to a stainless steel vacuum line and anhydrous CHF_3 was condensed into the vessel at -196 °C to a height of ca. 5 cm and the sample tube and the content were cooled to -196 °C and flame-sealed under vacuum. The reaction vessel was warmed in stages up to room temperature and maintained at 0 °C for 12 h. After cooling to -78 °C, a white, crystalline powder precipitated and the Raman spectra of the solid under frozen solvent was recorded at -160 °C (directly on the upper and lower regions of the sealed off portion of the thick-wall glass reaction vessel containing the solid sample), and confirmed that no reaction had occurred.

Equimolar amounts of $[\text{N}(\text{CH}_3)_4][\text{F}]$ (0.01474 g, 0.1582 mmol) and XeF_2 (0.02394 g, 0.1414 mmol) were added to a 4-mm o.d. FEP reaction vessel. Dry acetonitrile solvent was then added to the sample and reacted for ca. 1 h at -30 °C. The solvent was removed under vacuum at -30 °C and a Raman spectrum was recorded at -160 °C on the non-volatile residue, confirming that no reaction had occurred.

Cesium fluoride (0.08105 g, 0.5336 mmol) and XeF_2 (0.38827 g, 2.294 mmol) were loaded into a 4-mm o.d. FEP tube. The tube was then heat sealed under ca. 0.5 atm N_2 , and then immersed in an oil bath and heated to 145 °C. A Raman spectrum recorded at -155 °C confirmed that no reaction had occurred. A sample of $[\text{N}(\text{CH}_3)_4][\text{F}]$ (0.02076 g, 0.0223 mol) and XeF_2 (0.23772 g, 1.404 mmol) was similarly prepared. The sample was immersed in an oil bath and detonated violently at the melting point of XeF_2 (129 °C).

Nuclear Magnetic Resonance Spectroscopy. Single selective inversion experiments were conducted as previously described and the full observed relaxation,²¹ under the combined influence of spin-lattice relaxation and chemical exchange was analyzed using the CIFIT program.³⁵ Equimolar samples of XeF₂ and [N(CH₃)₄][F] were prepared in CH₃CN solvent with concentrations of 0.18 M and 0.36 M, as described previously.¹⁷

Fluorine-19 NMR spectra were referenced to external CFCI₃ at 30 °C. The NMR probe was cooled using a nitrogen flow and variable temperature controller (BV-T 2000). All spectra in this study were recorded unlocked without spinning the samples. The NMR spectra were recorded on a Bruker DRX-500 spectrometer and acquired at 470.560 MHz in 64 K memories over a 14.86 kHz spectral width corresponding to an acquisition time of 0.23 s and a data point resolution of 2.18 Hz/point.

Raman Spectroscopy. Low-temperature (−155 to −165 °C) Raman spectra were recorded on a Bruker RFS 100 FT Raman spectrometer using 1064-nm excitation as previously described.³⁶ Spectra were recorded in glass or ¼-in. FEP sample tubes using a laser power of 200 mW and a total of 300 scans.

Computational Methods. Molecular geometries were optimized with CCSD and DFT (using the PBE1PBE exchange-correlation functional) with aug-cc-pVTZ (F) and aug-cc-pVTZ-PP (Xe) basis sets (basis sets obtained from <https://bse.pnl.gov/bse/portal>). The nature of all stationary points found was assessed by performing frequency analyses. Calculations involving solvent effects were performed using the CPCM model³³ and employing the default parameters for CH₃CN. Natural atomic orbital and natural bond orbital analyses were conducted using the NBO 5.0 code;³⁷ electron localization function analyses were performed with the program package TopMod.³⁸ Visualizations of molecular structures and ELF isosurfaces were done with the gOpenMol program.^{39,40} Quantum-chemical calculations were carried out using the program

Gaussian 09⁴¹ for geometry optimizations, vibrational frequencies, and their intensities and the program Gaussian 03⁴² for NBO analysis.

Acknowledgements. We thank the Natural Sciences and Engineering Research Council of Canada for the award of a postgraduate scholarship (N.V.) and for support in the form of a Discovery Grant (G.J.S.). We also thank the Academy of Finland (H.T.) for financial support. This work is dedicated to the memory of Dr. Donald W. Hughes (1949-2010).

Supporting Information Available: Calculated gas-phase frequencies (cm^{-1}) and relative Raman intensities for the XeF_3^- and $\text{F}_2\text{Xe}^--\text{F}^-$ anions (Table S1); complete references 41 and 42.

References

- (1) Grant, D. J.; Wang, T.-H.; Dixon, D. A.; Christe, K. O. *Inorg. Chem.* **2010**, *49*, 261–270.
- (2) Christe, K. O.; Curtis, E. C.; Dixon, D. A.; Mercier, H. P. A.; Sanders, J. C. P.; Schrobilgen, G. J. *J. Am. Chem. Soc.* **1991**, *113*, 3351–3361.
- (3) Peacock, R. D.; Selig, H.; Sheft, I. *Proc. Chem. Soc.* **1964**, 285.
- (4) Peacock, R. D.; Selig, H.; Sheft, I. *J. Inorg. Nucl. Chem.* **1966**, *28*, 2561–2567.
- (5) Ellern, A.; Mahjoub, A.; Seppelt, K. *Angew. Chem., Int. Ed. Engl.* **1996**, *35*, 1123–1125.
- (6) Peterson, S. W.; Holloway, J. H.; Coyle, B. A.; Williams, J. M. *Science* **1971**, *173*, 1238–1239.
- (7) Adam, S.; Ellern, A.; Seppelt, K. *Chem. Eur. J.* **1996**, *2*, 398–402.
- (8) Christe, K. O.; Wilson, W. W. *Inorg. Chem.* **1982**, *21*, 4113–4117.
- (9) Ward, R. D. *J. Chem. Ed.* **1963**, *40*, 277–279.
- (10) Wilson, I. L. *J. Fluorine Chem.* **1975**, *5*, 13-18.
- (11) Liebman, J. F. *J. Fluorine Chem.* **1976**, *7*, 531–535.
- (12) Begun, G. M.; Compton, R. N. *Int. J. Mass Spectrom. Ion Phys.* **1979**, *30*, 379–382.

- (13) Studier, M. H.; Sloth, E. N. In *Noble Gas Compounds*; Hyman, H. H., Ed.; University of Chicago Press: Chicago, 1963, pp. 47–49.
- (14) Krouse, I. H.; Hao, C.; Check, C. E.; Lobring, K. C.; Sunderlin, L. S.; Wenthold, P. G. *J. Am. Chem. Soc.* **2007**, *129*, 846–852.
- (15) Misochko, E. Y.; Akimov, A. V.; Belov, V. A.; Tyurin, D. A. *Inorg. Chem.* **2009**, *48*, 8723–8728.
- (16) Appelman, E. H. *Inorg. Chem.* **1967**, *6*, 1268–1269.
- (17) Vasdev, N.; Pointner, B. E.; Chirakal, R.; Schrobilgen, G. J. *J. Am. Chem. Soc.* **2002**, *124*, 12863–12868.
- (18) Schrobilgen, G. J.; Firnau, G.; Chirakal, R.; Garnett, E. S. *J. Chem. Soc., Chem. Commun.* **1981**, 198–199.
- (19) Sood, S.; Firnau, G.; Garnett, E. S. *Int. J. Appl. Radiat. Isot.* **1983**, *34*, 743–745.
- (20) Firnau, G.; Chirakal, R.; Sood, S.; Garnett, E. S. *J. Labelled Compd. Radiopharm.* **1981**, *18*, 7–8.
- (21) Bain, A. D.; Cramer, J. A. *J. Magn. Reson. A.* **1996**, *118*, 21–27.
- (22) Christe, K. O.; Wilson, W. W. *J. Fluorine Chem.* **1990**, *46*, 339–342.
- (23) Dukat, W. W.; Holloway, J. H.; Hope, E. G.; Townson, P. J. *J. Fluorine Chem.* **1993**, *62*, 293–296.
- (24) Christe, K. O. *J. Fluorine Chem.* **1995**, *71*, 149–150.
- (25) Bartlett, N.; Yeh, S.; Kourtakis, K.; Mallouk, T. *J. Fluorine Chem.* **1984**, *26*, 97–116.
- (26) Shen, C.; Hagiwara, R.; Mallouk, T.; Bartlett, N. In *Inorganic Fluorine Chemistry, Toward the 21st Century*; Thrasher, J. S., Strauss, S. H., Eds.; ACS Symposium Series 555: Washington, DC, 1994; Chapter 2, pp. 26–39.
- (27) Jenkins, H. D. B.; Roobottom, H. K.; Passmore, J.; Glasser, L. *Inorg. Chem.* **1999**, *38*, 3609–3620.
- (28) Jenkins, H. D. B.; Tudela, D.; Glasser, L. *Inorg. Chem.* **2002**, *41*, 2364–2367.
- (29) Jenkins, H. D. B.; Glasser, L. *Inorg. Chem.* **2003**, *42*, 8702–8708.
- (30) Osborne, D. W.; Flotow, H. E.; Malm, J. G. *J. Chem. Phys.* **1972**, *57*, 4670–4675.

- (31) Jenkins, H. D. B.; Glasser, L.; Klapötke, T. M.; Crawford, M.-J.; Bhasin, K. K.; Lee, J.; Schrobilgen, G. J.; Sunderlin, L. S.; Liebman, J. F. *Inorg. Chem.* **2004**, *43*, 6238–6248.
- (32) Bondi, A. *J. Phys. Chem.* **1964**, *68*, 441–451.
- (33) Barone, V.; Cossi, M. *J. Phys. Chem. A* **1998**, *102*, 1995–2001.
- (34) Mercier, H. P. A.; Moran, M. D.; Sanders, J. C. P.; Schrobilgen, G. J.; Suontamo, R. J. *Inorg. Chem.* **2005**, *44*, 49–60.
- (35) Bain, A. D.; Duns, G. J.; Rathgeb, F.; Vanderkloet, J. *J. Phys. Chem.* **1995**, *99*, 17338–17343.
- (36) Gerken, M.; Dixon, D. A.; Schrobilgen, G. J. *Inorg. Chem.* **2000**, *39*, 4244–4255.
- (37) Glendening, E. D.; Badenhop, J. K.; Reed, A. E.; Carpenter, J. E.; Bohmann, J. A.; Morales, C. M.; Weinhold, F. *NBO 5.0*, Theoretical Chemistry Institute, University of Wisconsin: Madison, WI, 2001.
- (38) Noury, S.; Krokidis, X.; Fuster, F.; Silvi, B. *TopMod package*, University of Paris VI: Paris, 1998.
- (39) Laaksonen, L. *J. Mol. Graph.* **1992**, *10*, 33–34.
- (40) Bergman, D. L.; Laaksonen, L.; Laaksonen, A. *J. Mol. Graph. Model.* **1997**, *15*, 301–306.
- (41) Frisch, M. J. et al. *Gaussian 09 (Revision A.02)*, Gaussian, Inc.: Wallingford, CT, 2009.
- (42) Frisch, M. J.; et al. *Gaussian 03, (Revision D.01)*, Gaussian, Inc.: Wallingford CT, 2004.